High-Pressure Chemistry

DOI: 10.1002/anie.201001581

Pressure-Driven Assembly of Spherical Nanoparticles and Formation of 1D-Nanostructure Arrays**

*Huimeng Wu, Feng Bai, Zaicheng Sun, Raid E. Haddad, Daniel M. Boye, Zhongwu Wang, and Hongyou Fan**

Owing to their size- and shape-dependent properties,[1–3] nanoparticles have been successfully used as functional building blocks to fabricate multidimensional ordered assemblies for the development of "artificial solids" (e.g., metamaterials) with potential applications in nanoelectronic and optical devices.[4–8] Until now, the fabrication of ordered nanoparticle assemblies has relied on specific chemical or physical interparticle interactions, such as van der Waals interactions,[6] dipole–dipole interactions,[9] chemical reactions,[8,10,11] and DNA templating.[5,12,13] Consequently, self-assembly has involved the formation of higher-dimensional nanoparticle architectures from single nanoparticles. Herein, we report that a novel external pressure can be utilized to engineer nanoparticle assembly, to fabricate 1D metallic nanostructures and to form ultrahigh-density ordered 1D nanostructure arrays. Ordered films of spherical gold nanoparticles with a face-centered cubic (fcc) mesophase were compressed with a diamond anvil cell (DAC). In situ high-pressure small-angle X-ray scattering (HP SAXS) measurements showed that gradual elevation of the external pressure from ambient pressure to 8.9 GPa caused reversible shrinkage of the dimensions of the lattice unit cell and thus enabled the fine-tuning of interparticle spacing. Pressures between 8.9 and 13 GPa drove the nanoparticles to coalesce to form 1D nanostructures (nanorods or nanowires) and ordered hexagonal arrays of the nanostructures with *P6mm* symmetry. Dispersion of the ordered arrays in organic solvents resulted in uniform single nanostructures that could reassemble into ordered arrays upon evaporation of the solvent. This simple and efficient method enables the nanoengineering of nanoparticle assemblies for the fabrication of new complex nanoparticle architectures without reliance on specific chemical and physical interactions.[5,8–13]

We synthesized spherical gold nanoparticles by using a one-phase method and used dodecanethiol as the capping ligand (see details in the Supporting Information).[14] The gold nanoparticles had an average diameter of 5.2 nm with a standard deviation of 4.2%. The fcc ordered gold-nanoparticle polymer films were fabricated through a solvent-evaporation process on silicon wafers. When the ordered nanoparticle film was loaded into the DAC (a schematic illustration of the measurement is shown in Figure S1a of the Supporting Information),[15] it maintained the fcc mesophase, which exhibited a [110] orientation, as revealed by small-angle synchrotron X-ray scattering (SAXS) and microscope measurement. The SAXS pattern and integrated spectrum (see Figure S1b,c in the Supporting Information) collected at ambient pressure indicated a pattern specific to an fcc mesophase with the $Fm\bar{3}m$ space group. The unit-cell parameter a_{fcc} was calculated to be 104.0 Å. Representative SEM images (see Figure S1d,e in the Supporting Information) taken of the surface and cross-section of the gold-nanoparticle film verified that the film consisted of 3D ordered arrays. Both the electron-diffraction pattern (insets in Figure S1d,e) and fast Fourier transform (FFT) analysis (see Figure S2 in the Supporting Information) indicated that the gold nanoparticles are organized in a periodic and ordered fcc mesophase with a preferred orientation along the [110] direction.

The nanoparticle film was gradually compressed in the DAC from ambient pressure to 13 GPa at room temperature, and then the pressure was gradually released back to ambient pressure. The SAXS pattern and integrated spectrum of the resulting material (Figure 1a,b) are consistent with a 2D hexagonal mesophase with *P6mm* symmetry. The primary peaks were assigned as 100, 110, 200, 210, and 300 reflections.

Electron-microscopic images of the samples after release of the pressure from 13 GPa to ambient pressure (Figure 1c–f) showed that the ordered fcc spherical-nanoparticle superlattice had been converted into an ordered nanowire array (Figure 1c). The gold-nanowire array consisted of individual

[*] Dr. H. Wu, Prof. H. Fan
Sandia National Laboratories
Advanced Materials Laboratory,1001 University Blvd. SE
Albuquerque, NM 87106 (USA)
E-mail: hfan@sandia.gov
Homepage: http://www.unm.edu/~hyfan/

Dr. F. Bai, Dr. Z. Sun, R. E. Haddad, Prof. H. Fan
Center for Micro-Engineered Materials, Department of Chemical and Nuclear Engineering, University of New Mexico
Albuquerque, NM 87131 (USA)

Prof. D. M. Boye
Physics Department, Davidson College
Davidson, NC 28035 (USA)

Prof. Z. Wang
Cornell High Energy Synchrotron Source, Wilson Laboratory
Cornell University, Ithaca, NY 14853 (USA)

[**] The authors acknowledge Dr. Bryan Kaehr and Dr. Detlef-M. Smilgies for their comments. This research was supported by the US Department of Energy (DOE), the BES Program, the LDRD program of Sandia National Laboratory, and the NSF (DMI-0625897). The Cornell High Energy Synchrotron Source is supported by the NSF and NIH/NIGMS through NSF award DMR-0225180. Sandia is a multiprogram laboratory operated by Sandia Corporation, a Lockheed Martin Company, for the National Nuclear Security Administration of the US DOE under contract DE-AC04-94AL85000.

Supporting information for this article is available on the WWW under http://dx.doi.org/10.1002/anie.201001581.

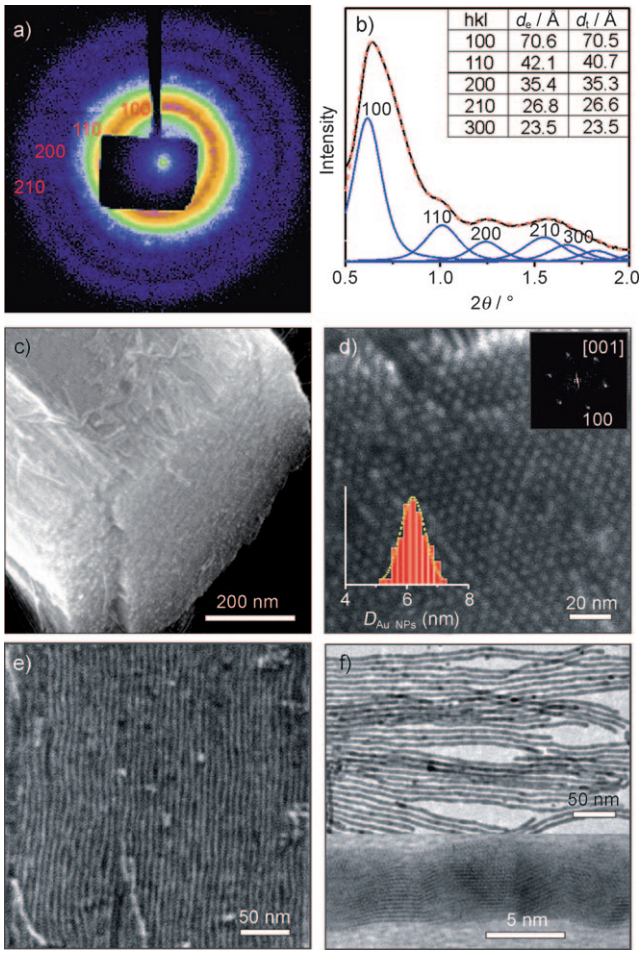

Figure 1. Structure of the gold nanowires and their ordered arrays. a) HP-SAXS image of the sample after release of the pressure. b) The SAXS spectrum integrated from the image in (a) with fitted peaks (red). The table compares the experimental (d_e) and theoretical d spacing (d_t) of different crystal planes. The d_t values were calculated on the basis of the parameter $a = 81.4$ Å in the space group *P6mm*. c) SEM image after release of the pressure from 13 GPa to ambient pressure. d) Plan-view SEM image taken along the nanowire *c*-axial direction. The insets show the size distribution (graph; NPs = nanoparticles) and the FFT pattern (top right) of the arrays. e) Cross-sectional SEM image taken from the direction perpendicular to the nanowire *c* axis. f) TEM images of the reassembled nanowire arrays after solvent evaporation.

gold nanowires with hexagonal close packing. Figure 1 d,e shows representative SEM images of the nanowire mesophases oriented along the [001] and [110] directions, respectively. The SEM images are consistent with a unit cell with a lattice parameter $a_{hex} = 81.4$ Å and a uniform minimum center-to-center spacing between nanowires of 8.1 nm. On the basis of the packing geometry, this value corresponds to an ultrahigh nanowire density of approximately 1.7×10^{12} nanowires per square centimeter.[16]

The two end facets of the nanowire bundles are very flat (Figure 1 c; see also Figure S3 in the Supporting Information), which suggests a constant length of the nanowires. Single nanowires were obtained by dispersion of the nanowire arrays in organic solvents (e.g., toluene). A TEM image of the nanowires (Figure 1 f) shows that they are uniform in diameter and length. The average diameter is 6.1 nm with a standard deviation of 4.6 %. The length is consistent with the distance between the two end faces and ranges from 400 nm to 1.5 μm, depending on the initial film thickness of the ordered nanoparticles. Short nanowires (or nanorods) were obtained from a thin film. High-resolution TEM imaging (Figure 1 f) revealed that the gold nanowires are polycrystalline. Along the *c* axis, each nanowire consists of crystalline nanodomains whose size is close to that of the original spherical gold nanoparticles. This result indicates that the gold nanowires are formed through the sintering of spherical gold nanoparticles along the nanowire *c* axis, as confirmed by TEM studies (see below). These individual nanowires can form stable colloidal dispersions in organic solvents and reassemble into ordered arrays upon solvent evaporation (Figure 1 f). Overall, our approach provides greater control than chemical methods[17–19] over the length of the nanowires and the formation of ordered, ultrahigh-density nanowire arrays.

To investigate the nanoparticle-assembly pathway and the nanowire-formation process, we carried out in situ HP-SAXS experiments to follow the structure evolution of the nanoparticle films during the compression and release processes. The HP-SAXS results suggest the formation of gold-nanowire arrays through a phase transformation from a 3D fcc mesophase to a 2D hexagonal nanowire mesophase. Before the formation of gold nanowires, the spherical-nanoparticle mesophase exhibits reversible unit-cell-dimension shrinkage. During this reversible process, the interparticle separation can be precisely controlled by external pressure. Figure 2 a,b shows representative HP-SAXS patterns and integrated spectra collected at varied compression and release pressures. At ambient pressure, the gold-nanoparticle film exhibits an fcc mesophase. In the range from ambient pressure to

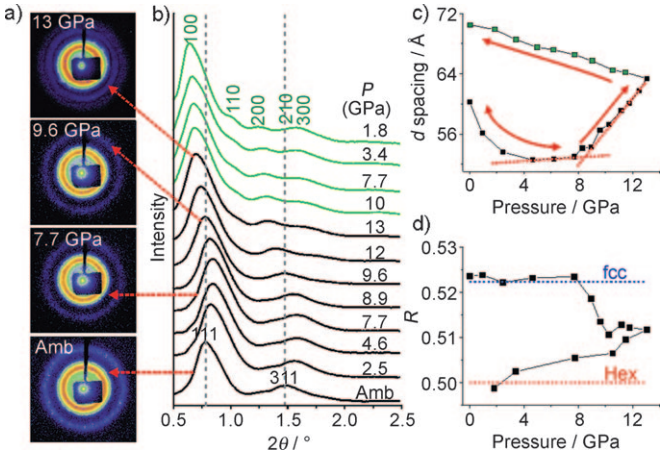

Figure 2. Structural evolution of gold-nanoparticle assemblies during compression and release. a) HP-SAXS patterns of gold-nanoparticle assemblies at ambient pressure, 7.7 GPa, 9.6 GPa, and 13 GPa. b) Integrated spectra derived from the HP-SAXS patterns at varied pressures during compression (black spectra) and release (green spectra). c) Graph showing the *d* spacing of the first Bragg reflection in each HP-SAXS spectrum in (b). The data points in green correspond to release of the pressure. d) Graph showing the *d*-spacing ratio (R) at different pressures.

8.9 GPa, HP-SAXS data indicate that the gold-nanoparticle assembly remains in the fcc structure with the [110] orientation. As the pressure increases to 8.9 GPa, all the HP-SAXS peaks shift slightly to higher 2θ values (lower d spacing), which indicates shrinkage in the unit-cell dimensions. When the pressure is gradually released, all peaks return to their starting positions. Thus, the change in the unit-cell dimensions is reversible between ambient pressure and 8.9 GPa.

This reversible behavior is further verified by the d-spacing changes (Figure 2c) and the constancy of the d-spacing ratio R at varying pressures (Figure 2d): Below 8.9 GPa, changes in the d spacing are reversible (as denoted by the bidirectional arrow in Figure 2c), and R remains constant and close to the theoretical value of $R = d_{311}/d_{111} = \sqrt{3/11} = 0.522$ for an fcc mesophase (Figure 2c). The lattice constant shrinks from 104 Å at ambient pressure to 91 Å at 8.9 GPa and returns to 103 Å when the pressure is completely released. Consequently, the interparticle separation distance along the [110] direction varies reversibly between 74 and 64 Å. Below 8.9 GPa, the nanoparticles are not connected: the closest center-to-center particle distance is 64.4 Å at 7.7 GPa; this distance is slightly larger than the 5.2 nm diameter of the gold nanoparticles.

The nanoparticle assembly exhibits an intermediate structure that cannot be assigned as either fcc or a 2D hexagonal mesophase during the pressure course: 8.9 GPa → 13 GPa → 7.7 GPa. The unit-cell-dimension changes are irreversible during this pressure course. All HP-SAXS peaks shifted to lower 2θ values (higher d spacing; Figure 2c) rather than undergoing a continuous shift to lower d spacings. This result suggests that a structure transformation had taken place. More importantly, the d-spacing ratio R decreased from the theoretical value of 0.522 to about 0.51 (Figure 2d), which further confirms a structural transformation. When the pressure was released to 7.7 GPa, all HP-SAXS peaks continued to shift to lower 2θ values instead of returning to their original positions. Below 7.7 GPa, the d-spacing ratio further decreased to about 0.5: the theoretical d_{200}/d_{100} ratio for a 2D hexagonal mesophase. The corresponding HP-SAXS patterns were also consistent with a 2D hexagonal mesophase.

Besides in situ HP SAXS, TEM experiments were performed to follow the nanostructure changes. Our TEM results further confirm that the gold nanowires are formed through spherical-nanoparticle sintering. Upon the exposure of gold nanoparticles to pressures above 8.9 GPa, we observed the formation of numerous gold-nanoparticle dimers, trimers, and nanorods (Figure 3a). TEM images (Figure 3a) indicated that the nanoparticles sintered together seamlessly along the nanowire c axis. This behavior distinguished the nanowires from previously reported 1D nanoparticle nanostructures in which the nanoparticles are connected through organic ligands that are chemically bonded to each neighboring nanoparticle.[8,11] TEM images indicated that the gold nanoparticles sintered under applied pressures greater than 8.9 GPa. Continuous compression along the [110] direction under pressures up to 13 GPa led to the formation of nanorods and nanowires. Oriented sintering under high pressure slightly increases the diameter of the final nanowires relative to that of the original nanoparticles.

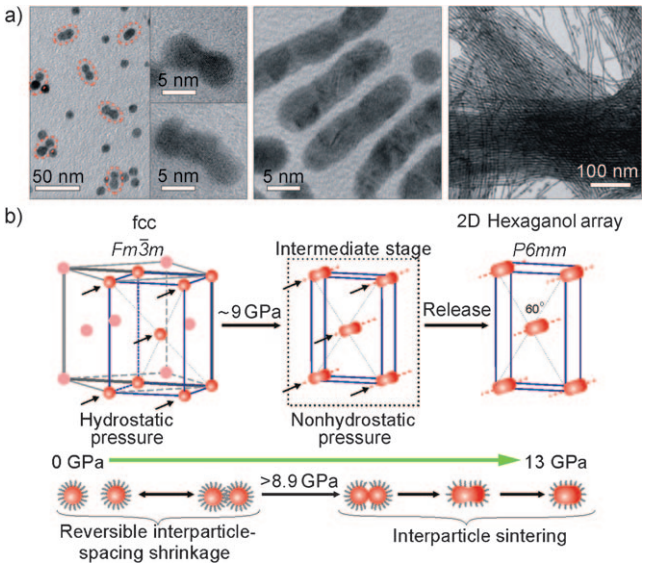

Figure 3. Proposed mechanism for the formation of 1D nanostructures. a) Representative TEM images of the sintered gold nanoparticles. b) Schematic model for the orientated sintering of gold nanoparticles into gold-nanowire arrays along the [110] direction under compression. The small arrows show the pressure direction.

Liquid silicone oil was used as the pressure-transmitting medium in our experiments. In general, it is capable of maintaining loaded samples in a hydrostatic environment under pressures up to about 9–10 GPa.[20,21] Above this threshold, the generation of deviatoric stress results in a pressure gradient oriented vertically across the sample. This nonhydrostatic stress can be evaluated through quantitative texture analysis by unraveling 2D HP-SAXS patterns (Debye–Scherrer rings) into Cartesian (cake) plots of the azimuthal angle as a function of 2θ.[22,23] We observed an evident waviness at pressures above 8.9 GPa (see Figure S4 in the Supporting Information) that is indicative of the generation of a nonhydrostatic stress field during compression of the nanoparticle film.

On the basis of these experimental results, the formation of well-ordered 1D metallic nanostructures and their ordered arrays can be understood as follows (Figure 3b): Below 8.9 GPa, the sample is compressed under a hydrostatic pressure field. The isotropic pressure applied uniformly through all directions to the nanoparticle assembly causes the dimensions of the fcc unit cell to shrink uniformly. The fcc mesophase and its [110] orientation are retained. For pressures above 8.9 GPa, a nonhydrostatic stress is generated and applied perpendicularly to the nanoparticle film. Owing to the [110] orientation of the nanoparticle mesophase, nanoparticles receive much greater stress along the [110] direction than along other crystallographic directions. Thus, nanoparticle sintering occurs preferentially along the [110] direction. Continuous compression to 13 GPa drives the spherical nanoparticles to touch and finally sinter into 1D nanostructures (nanorods and nanowires) along the [110] direction (Figure 3b). Ultimately, bundles (or arrays) of well-oriented nanowires with their c axis along the former fcc [110] direction are formed.

In summary, we have demonstrated that the pressure-induced phase transformation of a nanoparticle assembly provides a new route for the engineering of nanoparticle architectures and the fabrication of new nanostructured materials. The reversible changes in the nanoparticle-unit-cell dimensions under pressure enable the precise control of interparticle separation in 2D or 3D nanoparticle assemblies and thus offers unique robustness for the investigation of both quantum and classic coupling interactions.[2] A fundamental understanding of nanoparticle assembly under pressure would provide useful insight for material integration through pressure-driven nanofabrication processes, such as the embossing process: a key process for the fabrication of micro-/nanooptical and electronic devices.[24]

Received: March 16, 2010
Revised: June 14, 2010
Published online: July 28, 2010

Keywords: high-pressure chemistry · nanostructures · phase transitions · self-assembly · small-angle X-ray scattering

[1] A. P. Alivisatos, *Science* **1996**, *271*, 933.
[2] C. P. Collier, R. J. Saykally, J. J. Shiang, S. E. Henrichs, J. R. Heath, *Science* **1997**, *277*, 1978.
[3] H. Zeng, J. Li, J. P. Liu, Z. L. Wang, S. H. Sun, *Nature* **2002**, *420*, 395.
[4] H. Y. Fan, K. Yang, D. M. Boye, T. Sigmon, K. J. Malloy, H. F. Xu, G. P. Lopez, C. J. Brinker, *Science* **2004**, *304*, 567.
[5] S. Y. Park, A. K. R. Lytton-Jean, B. Lee, S. Weigand, G. C. Schatz, C. A. Mirkin, *Nature* **2008**, *451*, 553.
[6] C. B. Murray, C. R. Kagan, M. G. Bawendi, *Science* **1995**, *270*, 1335.
[7] S. H. Sun, C. B. Murray, D. Weller, L. Folks, A. Moser, *Science* **2000**, *287*, 1989.
[8] G. A. DeVries, M. Brunnbauer, Y. Hu, A. M. Jackson, B. Long, B. T. Neltner, O. Uzun, B. H. Wunsch, F. Stellacci, *Science* **2007**, *315*, 358.
[9] Z. Y. Tang, N. A. Kotov, M. Giersig, *Science* **2002**, *297*, 237.
[10] J. G. Worden, A. W. Shaffer, Q. Huo, *Chem. Commun.* **2004**, 518.
[11] K. M. Sung, D. W. Mosley, B. R. Peelle, S. G. Zhang, J. M. Jacobson, *J. Am. Chem. Soc.* **2004**, *126*, 5064.
[12] J. Sharma, R. Chhabra, A. Cheng, J. Brownell, Y. Liu, H. Yan, *Science* **2009**, *323*, 112.
[13] H. Yan, S. H. Park, G. Finkelstein, J. H. Reif, T. H. LaBean, *Science* **2003**, *301*, 1882.
[14] N. Zheng, J. Fan, G. D. Stucky, *J. Am. Chem. Soc.* **2006**, *128*, 6550.
[15] H. K. Mao, P. M. Bell, *Science* **1978**, *200*, 1145.
[16] R. Beckman, E. Johnston-Halperin, Y. Luo, J. E. Green, J. R. Heath, *Science* **2005**, *310*, 465.
[17] C. Wang, Y. J. Hu, C. M. Lieber, S. H. Sun, *J. Am. Chem. Soc.* **2008**, *130*, 8902.
[18] Z. Y. Huo, C. K. Tsung, W. Y. Huang, X. F. Zhang, P. D. Yang, *Nano Lett.* **2008**, *8*, 2041.
[19] X. M. Lu, M. S. Yavuz, H. Y. Tuan, B. A. Korgel, Y. N. Xia, *J. Am. Chem. Soc.* **2008**, *130*, 8900.
[20] Q. X. Guo, Y. S. Zhao, W. L. Mao, Z. W. Wang, Y. J. Xiong, Y. N. Xia, *Nano Lett.* **2008**, *8*, 972.
[21] D. D. Ragan, D. R. Clarke, D. Schiferl, *Rev. Sci. Instrum.* **1996**, *67*, 494.
[22] L. Miyagi, S. Merkel, T. Yagi, N. Sata, Y. Ohishi, H. R. Wenk, *J. Phys. Condens. Matter* **2006**, *18*, S995.
[23] G. Ischia, H. R. Wenk, L. Lutterotti, F. Berberich, *J. Appl. Crystallogr.* **2005**, *38*, 377.
[24] S. R. Quake, A. Scherer, *Science* **2000**, *290*, 1536.

